PERGAMON

Solid-State Electronics 44 (2000) 1135–1143

SOLID-STATE ELECTRONICS

Hydrodynamic modeling of avalanche breakdown in a gate overvoltage protection structure

Martin Knaipp [a,*], Werner Kanert [b], Siegfried Selberherr [c]

[a] *Austria Mikro Systeme International AG Schloß Premstätten, A-8141 Unterprem Stätten, Austria*
[b] *Infineon Technologies AG, AIAPTDCD Balanstrasse 73, D-81541 Munich, Germany*
[c] *Institute for Microelectronics, Gusshausstrasse 25-29, A-1040 Vienna, Austria*

Received 30 September 1999; received in revised form 19 January 2000; accepted 27 February 2000

Abstract

The breakdown of an overvoltage protection structure is analyzed in the temperature range from 298 to 523 K. The avalanche generation rates are modeled as a function of the carrier and lattice temperature. The generation rates are proportional to the carrier concentration. Careful attention is given to the pre-breakdown regime and to the breakdown process. The importance of various generation processes to the impact process is studied as well as the influence on variations of the ionization threshold energy and of the energy loss during the impact process. It is shown that the carrier generation inside the junction causes adiabatic carrier cooling, which leads to different carrier heating effects at low and high lattice temperature. The behavior of carrier heating at room temperature is strongly affected by the asymmetric field distribution inside the junction. The reason for this is the field dependence of the used trap assisted band to band tunneling model and of the direct band to band tunneling model. It is shown that at room temperature, the onset of hole impact ionization plays an important role for the electron heating. This is different at a temperature of 523 K, where the electrons dominate the onset of impact ionization. © 2000 Elsevier Science Ltd. All rights reserved.

Keywords: Impact ionization; Hydrodynamics; Avalanche breakdown; Avalanche diodes; Zener diodes

1. Introduction

In recent years, device feature sizes have been continuously scaled down to the sub-micron range. This size reduction causes an increase of the maximum field strength inside the device, which leads to a higher probability for avalanche processes. An example of investigations on impact ionization (II) is the substrate current simulation in MOSFETs, where the amount of substrate current is an important indicator for the aging behavior of the device [1,8].

To simulate the device breakdown, it is necessary to apply an accurate, physically motivated impact ionization model. The standard drift diffusion (DD) equations can only use a field dependent impact ionization model, as only inaccurate estimations of the carrier temperatures are available [2,3]. However, the electric field dependence is inaccurate, especially in small devices. Non-local effects must be taken into account when the typical thickness of space charge regions becomes comparable with the carrier energy relaxation lengths.

To account for non-locality in a more suitable way, the impact generation rate must be calculated as a function of the local carrier temperatures and not of the local electric field. The local carrier temperature can be calculated using Monte Carlo or hydrodynamic (HD) simulations.

One way to use the information of the average carrier temperature is to compute an equivalent electric field using the temperature versus electric field characteristic that results from Monte Carlo calculations for the homogeneous case [4–6]. Finally, the equivalent electric

* Corresponding author. Address: AMS International, Schloss Premstaetten, 8141 Unter-praemstaetten, Austria.

E-mail address: martin.knapp@amsint.com (M. Knaipp).

0038-1101/00/$ - see front matter © 2000 Elsevier Science Ltd. All rights reserved.
PII: S0038-1101(00)00046-0

Nomenclature

Γ_ν	electron and hole field enhancement factors
$\delta E_c, \delta E_v$	band edge displacements due to band gap narrowing
κ_n	electron heat conductivity
μ_n	electron mobility
$\mu_\nu(T_L, N_{tot})$	electron and hole mobilities depending on the lattice temperature and the total dopant concentration (independent of thermal carrier energies)
$\mu_\nu^{HD}(T_L, T_\nu)$	electron and hole hydrodynamic mobilities (depending on the thermal carrier energies)
$\nu = n, p$	electron and hole concentrations
ψ	local potential
$\tau_{w,\nu}$	electron and hole energy relaxation times
$\tau_\nu(T_L)$	electron and hole lifetimes (for the used recombination model)
τ_ν^0	electron and hole lifetimes at 300 K (for the used recombination model)
$\tau_{T_L,\vec{E}}$	electron and hole lifetimes depending on the lattice temperature and the electric field
D_n	electron diffusion coefficient
E_c	electron band edge energy
E_g	local band gap
E_t	energy level for the recombination centers
E_{thr}	threshold energy for impact ionization
$G^{SRH,TBB}$	generation rate for the combined Shockley–Read–Hall and trap assisted band to band tunneling processes
G^{BB}	generation rate for the band to band tunneling process
G_ν^{II}	electron and hole generation rates for the impact ionization process
H_n	electron heat source term
$\vec{J}_n$	electron current density
N_c, N_v	densities of states in the conducting and valence band
N_t	concentration of recombination centres
N_{tot}	total dopand concentration
N_{ref}	reference concentration for the band gap narrowing model
$\vec{S}_n$	electron energy flux
T_n	electron temperature
T_L	lattice temperature
c_n	electron scattering coefficient
c_ν^0	electron and hole capture rates (for the used recombination model)
k_B	Boltzmann constant
n_i	intrinsic concentration
q	elementary charge
$\vec{v}_{sat,\nu}$	electron and hole saturation velocities
w_n	electron average thermal energy

field is used instead of the local electric field to calculate the carrier generation rates. This is often performed in combination with a conventional DD model to achieve better convergence compared to a fully HD simulation [7].

The simulations in this paper have been carried out by applying a direct HD-II model, where the ionization rate per carrier depends only on the carrier temperature. For the simulations, the general purpose device simulator MINIMOS-NT is used where a consistent HD equation set is implemented. The usage of one type of simulator without any device specific Monte Carlo information is a common practise in industry. The advantage of the HD-II model compared to a DD-II model is its non-locality. This allows us to obtain the maximum generation rates per carrier at different device locations. The calculated generation rate per carrier and time depends on the local thermal energy, which results from an energy integration up to the local point.

As mentioned a typical application for impact ionization simulation is the reliability analysis of MOSFETs. The main difference between the reliability simulation and the breakdown simulation of a diode concerns the high multiplication factor of the diode after breakdown. The large number of generated carriers has influence on the potential distribution, which changes the device behavior. As a consequence, a robust numerical iteration scheme is necessary to achieve smooth generation rates over the device area. The high local fields require a high doping, which results in a steep junction. Therefore, additional models such as band gap narrowing, Shockley–Read–Hall generation (SRH), trap assisted band to band tunneling (TBB) and direct band to band tunneling (BB) have to be taken into account. After breakdown Auger recombination becomes important. In the pre-breakdown regime, the SRH, TBB and BB models generate free carriers in the depletion zone. This results in carrier cooling, which has an influence on the breakdown voltage. After breakdown, these models provide recombination as

$$np > n_i^2. \tag{1}$$

This paper is organized as follows:

In Section 2, the overvoltage protection structure is presented. Section 3 describes the used HD equation set together with the used models. Section 4 gives a discussion of the simulation results. In Section 5, conclusions are drawn.

2. The investigated device

The structure is widely used to protect electronic components, e.g. gates of MOSFETs, against voltage spikes. During operation, the anode contact is connected with the gate metal while the source is connected with the cathode. In the case of a gate voltage spike, the breakdown of the emitter p^+ protects the MOSFETs against overvoltage.

The top view of the emitter p^+ junction has an octagonal layout with an area of about 120 μm^2. The symmetrical line is shown on the left side of Fig. 1. The generated current is transferred through the p-well to an adjacent p^+ area, where the cathode contact is located. During device operation, the n-doped substrate is reverse biased. The applied cathode-substrate voltage is 10 V. Due to the high applied substrate voltage and the relatively low doped regions, the substrate p-well and substrate p^+ space charge region are much larger compared to the steep emitter p^+ junction. The measured currents which are scaled according to the simulated device area are shown in Fig. 2.

In a first step, we have to extract the amount of leakage current from the epitaxy/p-well and the epitaxy/p^+ space charge regions. This is necessary to estimate the influence of the SRH contribution in the breakdown junction. The pure SRH contribution is given in an operation regime, where the measured leakage current is almost independent of the applied voltage. This situation occurs in the high lattice temperature regime as shown in Fig. 2. The used SRH model is described in Ref. [9] with a lattice temperature dependence as given in Section 2. The SRH current in the epitaxy/p-well and epitaxy/p^+ space charge regions is only one part of the complete leakage current. The second part comes from the minority carrier concentration, which controls the diffusion current over the reverse pn-junction. This concentration is determined by a relatively small SRH contribution, which is generated outside the space charge regions and by a larger part, which is caused by the intrinsic concentration. It should be mentioned that the extraction of the SRH contribution was done by a complete two-dimensional simulation with appropriate boundary modeling using a device structure according to Fig. 1. The simulation results give best agreement with the measured 523 K data at a trap concentration of 5×10^{12} cm^{-3}. This concentration is then used for the one-dimensional device simulation of the emitter p^+ breakdown junction.

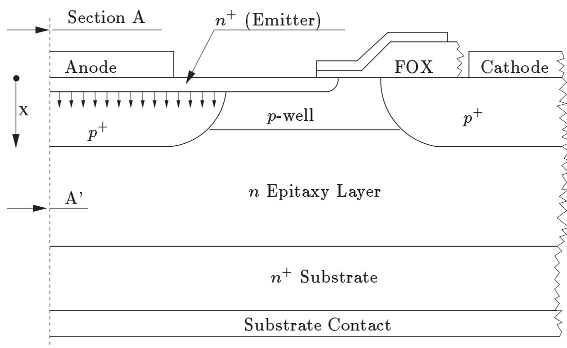

Fig. 1. The simulated overvoltage protection structure. The arrows indicate the break-down region. During operation the substrate bias is 10 V. The doping profile of Section A–A′ is used for the one-dimensional simulations. The arrow marked with x gives the positive x-direction.

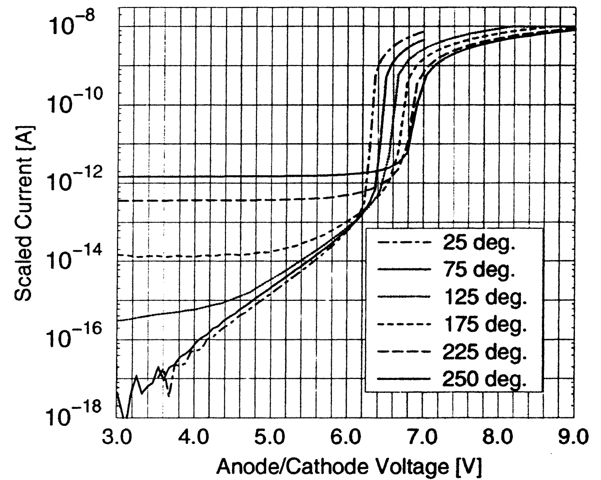

Fig. 2. Measured currents in a temperature range from 298 to 523 K. The current is scaled to 0.0012 μm^2 according to the size of the simulated device.

The result of the subtraction of the SRH component from the measured data is shown in Fig. 3.

The leakage currents in the pre-breakdown regime are now field dependent and nearly independent of the lattice temperature. It should be mentioned that the calibrated SRH contribution in the high temperature regime slightly overestimates the low temperature SRH contribution as described in Ref. [9]. This overestimation compensates the intrinsic current contribution, which finally leads to pure field dependent leakage current components. The field dependent leakage current in the pre-breakdown regime is therefore caused by the TBB, BB, and HD-II processes.

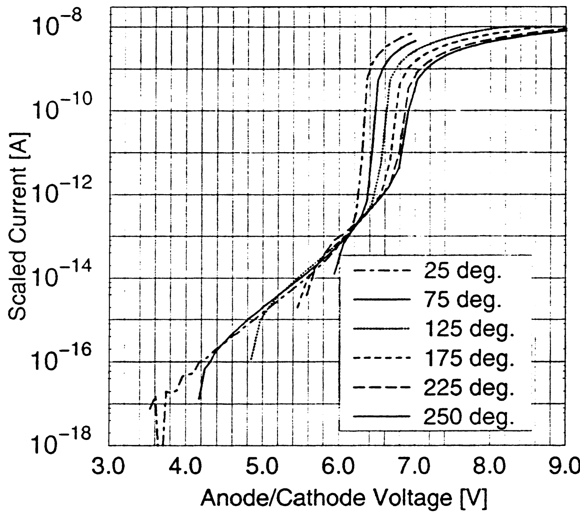

Fig. 3. Measured currents in a temperature range from 298 to 523 K with the sub-tracted SRH contribution which is calculated from a two-dimensional device simulation. The current is scaled to 0.0012 μm^2 according to the size of the simulated device.

3. Models and hydrodynamic equations

The Poisson and continuity equations for the HD equation set are straight forward and can be found, e.g. in Ref. [10]. Important for the considered problem is the formulation of the carrier energy flux equation, which reads for electrons (analog for holes)

$$\mathrm{div}\ \vec{S}_n = \mathrm{grad}\left(\frac{E_c}{q} - \psi\right)\vec{J}_n - \frac{3}{2}k_B n \frac{T_n - T_L}{\tau_{w,n}} + H_n. \quad (2)$$

The energy flux $\vec{S}_n$ is the sum of a conductive and convective term

$$\vec{S}_n = -\kappa_n\ \mathrm{grad}\ T_n - \frac{\vec{J}_n}{q}\ (w_n + k_B T_n). \quad (3)$$

For the heat conductivity κ we use the Wiedemann–Franz law

$$\kappa_n = (5/2 + c_n)\frac{k_B^2}{q}\ \mu_n n T_n = (5/2 + c_n) k_B D_n n. \quad (4)$$

For the simulation the scattering coefficients c_n and c_p are assumed to be zero.

The variable H_n in Eq. (2) is a heat source term of the carrier energy system. The term describes the net energy loss caused by the generation/recombination processes. In our simulations, it is assumed that in the pre-breakdown regime the SRH, TBB and BB models generate carriers with an energy close to the band edge. The generated carriers therefore have a temperature near the lattice temperature, which implies that the heat source term can be neglected for these processes. Only the continuity equations are involved without any energy loss in the carrier heat flux equation (2). After breakdown, the generation processes are replaced by the appropriate recombination processes and the question is how to split the recombination heat between the carrier and the lattice system. At least the influence of the recombination heat is small in the vicinity of the pn-junction because of the small density of recombination centers, hence the influence of this carrier heating process can be neglected. The important contribution to H_v is given by the II process itself, where the threshold energy E_{thr} has to be supplied by the carriers performing the ionization process. The carrier energy loss depends on the II generation rates for electrons and holes G_v^{II}:

$$H_v = G_v^{\mathrm{II}}\ E_g \quad (5)$$

In Eq. (5), the threshold energy E_{thr} is replaced by the local band gap energy E_g . The model for the band gap depends on the lattice temperature according to Ref. [11] and accounts for band gap narrowing [12]

$$\delta E_v = -\delta E_c = E_{\mathrm{ref}}\left(h + \sqrt{h^2 + 0.5}\right), \quad h = \ln(N_{\mathrm{tot}}/N_{\mathrm{ref}}) \quad (6)$$

with $N_{\mathrm{ref}} = 10^{17}$ cm^{-3} and $E_{\mathrm{ref}} = 0.009$ eV. For the carrier type v, a temperature dependent mobility model is used [13]

$$\mu_v^{\mathrm{HD}}(T_L, T_v) = \frac{\mu_v(T_L, N_{\mathrm{tot}})}{1 + \alpha(T_v - T_L)}, \quad \alpha = \frac{3}{2}\frac{k_B\ \mu_v(T_L, N_{\mathrm{tot}})}{\tau_{w,v}\ \vec{v}^2_{\mathrm{sat},v}\ q}. \quad (7)$$

The most important parameters, which have influence on the carrier temperatures are the energy relaxation times (ERT) $\tau_{w,v}$.

To estimate the influence of these times, we used two different models during the simulations. In the first model, we used the constant values of $\tau_{w,n} = 0.35$ ps for electrons and $\tau_{w,p} = 0.4$ ps for holes [14].

The second model evaluates the electron ERT, according to Ref. [15] with a lattice temperature dependence as described in Ref. [16]. In this model, the electron ERT increases from $\tau_{w,n} = 0.4$ ps for $T_n =$ 300 K up to more than $\tau_{w,n} = 0.8$ ps for $T_n > 6000$ K. The used lattice temperature dependence is described in Ref. [16] and results in a slightly ERT decrease at higher lattice temperatures. The equation for the electron ERT in picoseconds reads

$$\tau_{w,n}(T_n, T_L) = 1.0 - 0.538\exp\left[0.0015\left(\frac{T_n}{300\ \mathrm{K}}\right)^2 - 0.09\ \frac{T_n}{300\ \mathrm{K}} + 0.17\frac{T_L}{300\ \mathrm{K}}\right]. \quad (8)$$

The ERT for holes was extracted from Ref. [15] with the indirect method described in Ref. [16]. The results show that the hole ERT is nearly independent from the hole energy and the lattice temperature. During our simulations, we used a hole ERT of $\tau_{w,p} = 0.3$ ps.

The simulation results in Section 4 refer to the initial ERT models, where constant ERTs are used. The results of the simulations with the electron ERT of model 2 show a similar behavior. Section 4 shows that the average electron temperature is about 2500 K, which corresponds to an electron ERT of 0.6 ps. The section explains that the maximum carrier heating occurs at higher lattice temperatures, which results in a bigger carrier heating difference when different ERT models are used. The used coefficients for the HD-II model with respect to the two ERT models are summarized in Table 1.

The lattice temperature dependence of the SRH model is given in the exponents of the auxiliary variables n_1 and p_1, where the trap level E_t is assumed to equal the intrinsic level ($E_t - E_i = 0$ eV). In the pre-breakdown regime the number of available traps is much larger than the number of carriers involved in the generation process. Therefore the time of readjustment of an electron in a trap, once it is trapped, has been assumed to be negligible [3]. The model for the generation rate reads

$$
\begin{aligned}
G^{\mathrm{SRH,TBB}} &= -\frac{np - n_i^2}{\tau_p(n+n_1) + \tau_n(p+p_1)}, \\
n_1 &= N_c(T_L)\, e^{(-E_c+E_t)/kT_L}, \\
p_1 &= N_v(T_L) e^{(-E_t+E_v)/kT_L}.
\end{aligned} \tag{9}
$$

The lattice temperature dependence on the SRH lifetimes is expressed as a power law [17]. The lifetimes τ_ν are calculated using the lifetimes τ_ν^0 at 300 K

$$
\tau_\nu^0 = \frac{1}{c_\nu^0 N_t}, \quad \tau_\nu(T_L) = \tau_\nu^0 \left(\frac{300}{T_L}\right)^{1.5}. \tag{10}
$$

The trap assisted band to band tunneling model modifies the SRH lifetimes in Eq. (9) with the so-called field enhancement factors Γ_n and Γ_p. In case of strong local electric fields, the lifetimes in Eq. (9) are modified to

$$
\tau_\nu(T_L, \vec{E}) = \frac{\tau_\nu(T_L)}{1 + \Gamma_\nu(T_L, \vec{E})}. \tag{11}
$$

The factors Γ_n and Γ_p are evaluated according to Refs. [18,19].

In the pre-breakdown regime at a low lattice temperature, the BB process has a major influence. The model for the generation rate reads [19]

$$
G^{\mathrm{BB}} = -BD(n,p,n_i)\frac{|\vec{E}|^{2.5}}{E_g^{1/2}} \exp\left(-\frac{E_1 E_g^{3/2}}{|\vec{E}|}\right). \tag{12}
$$

The dependence on the lattice temperature is introduced via the band gap energy. The parameters B and E_1 were calibrated to the measured data and have the values $B = 1.5 \times 10^{17}\ \mathrm{s^{-1}\,cm^{-3}}$ and $E_1 = 2.25 \times 10^7\ \mathrm{V\,cm^{-1}}$. The relative population function $D(n,p,n_i)$ in Eq. (12) decides whether generation or recombination occurs

$$
D(n,p,n_i) = \frac{np - n_i^2}{(n+n_i)(p+n_i)}. \tag{13}
$$

The used HD-II model was first proposed in Refs. [20,21]. The generation rate $G(T_\nu, \nu)$ depends on the carrier temperature T_ν and is proportional to the carrier concentration ν

$$
\begin{aligned}
G_\nu^{\mathrm{II}}(T_\nu, \nu) &= \nu A\left[\left(1 + \frac{1}{2}u\right) \mathrm{erfc}\left(\frac{1}{\sqrt{u}}\right) - \frac{1}{2}\sqrt{u}\ \exp\left(\frac{-1}{u}\right)\right], \\
u &= \frac{k_B T_\nu}{E_{\mathrm{thr}}}.
\end{aligned} \tag{14}
$$

The lattice temperature dependence is introduced by rewriting Eq. (14) as

$$
\begin{aligned}
G_\nu^{\mathrm{II}}(T_\nu, T_L, \nu) &= \nu A(T_L, u)\left[\left(1 + \frac{1}{2}u\right) \mathrm{erfc}\left(\frac{1}{\sqrt{u}}\right) - \frac{1}{2}\sqrt{u}\ \exp\left(\frac{-1}{u}\right)\right], \\
u &= \frac{k_B T_\nu}{E_g(T_L, N_{\mathrm{tot}})}.
\end{aligned} \tag{15}
$$

For the pre-factor A, we take the relation,

$$
A(T_L, u) = C_1 \exp\left(C_2 \frac{T_L}{T_0}\right) \times \exp\left(\frac{E_{\mathrm{thr}}}{k_B T_0}\left(C_3 - C_4 \frac{T_L - T_0}{T_0}\right) u(T_\nu)\right). \tag{16}
$$

The coefficients C_1 to C_4 are summarized in Table 1. In Eq. (16), the reference temperature is $T_0 = 300$ K, and the ionization energy is $E_{\mathrm{thr}} = 1.12$ eV.

Table 1
The coefficients of the HD-II model[a]

	First ERT model	Second ERT model
C_1	$1.049 \times 10^8\ \mathrm{s^{-1}}$	$1.605 \times 10^8\ \mathrm{s^{-1}}$
C_2	3.823	3.823
C_3	0.34633	0.34633
C_4	0.0922	0.12

[a] The coefficients refer to the ERT models as explained in Section 3.

4. Simulation results

With the models described in the previous section, we simulated the one-dimensional device according to the vertical doping profile section A–A′ shown in Fig. 1. When we compare the simulation results of Fig. 4 with those of Fig. 3, a difference in the pre-breakdown regime is observed, which results from neglecting the SRH and the intrinsic contribution of the breakdown junction leakage current in Fig. 3.

One important question arises, why does the breakdown voltage increase with the lattice temperature? It can be shown that the breakdown condition is delayed when the lattice temperature is increased. The breakdown condition occurs when both carrier types reach a certain temperature so that avalanche generation can start.

The major part of this section explains the process of carrier heating within the breakdown junction. To understand the processes in the junction, it is convenient to look first at a typical field distribution. The electric field before breakdown with an applied bias of 6.3 V is shown in Fig. 5. The higher n-doped side (on the left) causes an asymmetric field inside the junction.

In Fig. 6, the carrier temperature distributions of the junction are shown at lattice temperatures of 298 and 523 K. To analyze the different generation models, we first show the simulation results with the SRH model, while the TBB, BB and HD-II models are neglected. It can be seen that the carrier temperatures at 523 K are higher than at the room temperature. This effect can be explained by comparing the diffusion current component and the SRH current component, which is generated in the junction space charge region. At a lattice temperature of 298 K, the SRH current is about 92 times larger than the diffusion current. The carrier temperature difference between 298 and 523 K can therefore be ex-

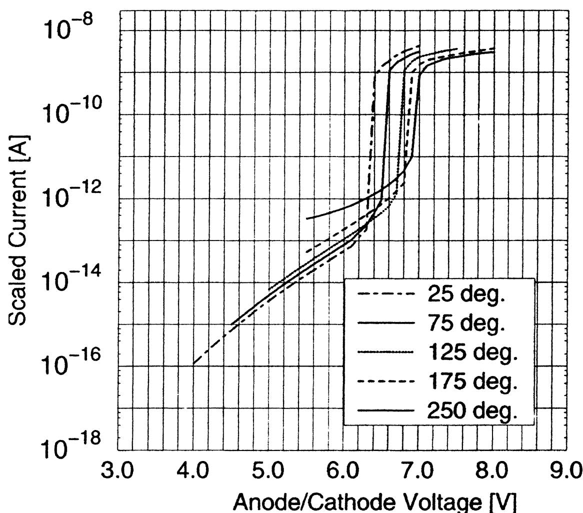

Fig. 4. Simulated currents with the described HD model. The currents in the pre-breakdown regime are smaller compared to Fig. 2 because the SRH contribution from epitaxy/p-well and the epitaxy/p^+ space charge regions is not included. On the other hand, the currents in the pre-breakdown regime are larger compared to Fig. 3 because the SRH contribution and the intrinsic contribution of the breakdown junction leakage currents are neglected in Fig. 3. The current is scaled to 0.0012 μm^2 according to the size of the simulated device.

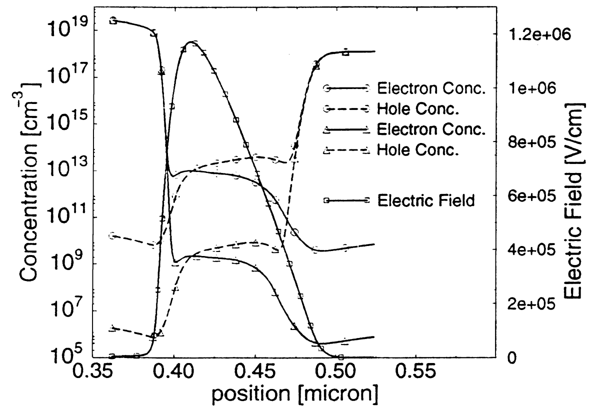

Fig. 5. The carrier concentrations at 298 K. The curves marked with triangles denote the concentrations before breakdown (bias 6.3 V). The curves with circles denote the concentrations after breakdown (bias 6.4 V). The position of maximum electron generation is at 0.41 μm and cause the increase in the hole concentration. The increase in the electron concentration at 0.46 μm is caused by the maximum hole generation rate at this position. The field strength at the bias of 6.3 V is also shown.

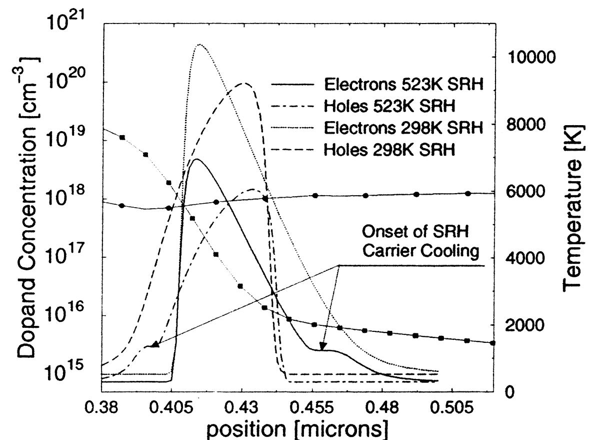

Fig. 6. Carrier heating of the investigated device using an anode (left side) bias of 4 V. Only SRH generation is considered. The electrons move from the right to the left. The donor doping is marked with the squared marks while the acceptor doping with the circled marks.

plained by a carrier cooling at 298 K inside the space charge region of the junction. This process is purely adiabatic as no energy loss occurs in the considered carrier system.

The resulting carrier heating is stronger when the entering current component gets higher. In contrast, the resulting carrier heating decrease when the generation of carrier inside the junction increase.

At the beginning of the space charge region, the carrier concentration caused by SRH generation is higher compared to the carrier density from the incoming diffusion current. This leads to a temperature decrease at the beginning of the carrier heating inside the junction (denoted by the arrows in Fig. 6). At a higher lattice temperature, the situation is completely different. As the temperature dependence of the diffusion current is proportional to n_i^2, the diffusion current increases much faster at higher temperatures than the SRH current, as the SRH current is only proportional to n_i (9). At 523 K, almost the total current is due to diffusion, so that nearly all carriers have to pass the whole space charge region, which finally leads to a higher carrier temperature.

In the next simulation, the process of TBB generation is switched on together with the SRH process. The results for 298 K are shown in Fig. 7. The maximum of the TBB generation rate is about 10 times higher compared to the maximum SRH rate. Due to the asymmetric junction, the field dependent process is located closer to the n-doped side. This asymmetry has an important influence on the final temperature dependence. The electrons are accelerated from the right to the left. When they arrive at the region where TBB occurs, they are cooled down by the generated electrons. The maximum electron temperature is therefore smaller compared to the pure SRH process. The situation is completely different for holes. When they enter the junction region, they are cooled by the generated TBB holes. The cooling process of the holes has its maximum at the beginning of their way through the junction.

Therefore, the relative part caused by the generated SRH holes in relation to the total number of generated holes is smaller compared with the result where only SRH generation is considered.

For that reason, the holes are heated more compared to the pure SRH process as shown in Fig. 6. The results of the simulations explain that the process of adiabatic cooling can finally lead to higher carrier temperatures at other locations.

In the following simulations, the additional process of BB generation is switched on. The results for 298 K are shown in Fig. 8. The maximum BB rate is about four orders of magnitude higher compared with the maximum TBB rate and much more localized on the left side of the junction. The generation process leads to a strong electron cooling and an additional hole heating. Until now, the simulation results overestimated the final temperature difference between electrons and holes because of the strong field dependence of the TBB and BB models. When the carrier temperature dependent HD-II model is switched on, the situation gets reversed because the holes start generating electron hole pairs at the right part of the pn-junction. The generated holes leave the junction at the right side. The generated electrons have to pass nearly the whole junction, which results in a rise of the electron temperature as shown in Fig. 8. The breakdown finally starts when the hole impact ionization has heated up the electron system above the breakdown temperature.

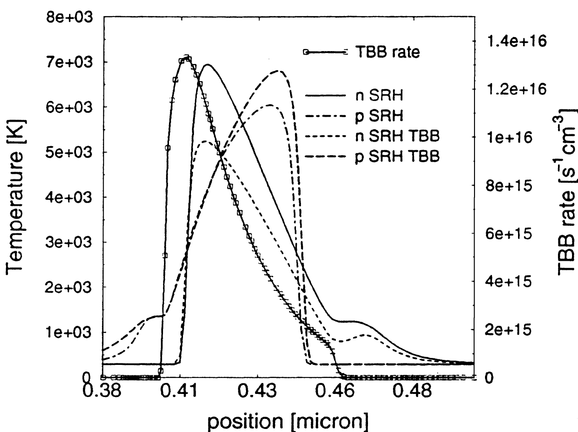

Fig. 7. Carrier heating of the investigated device using an anode (left side) bias of 4 V. Only SRH and TBB generation is considered. The electrons move from the right to the left. The linear shape of the TBB generation rate is also shown.

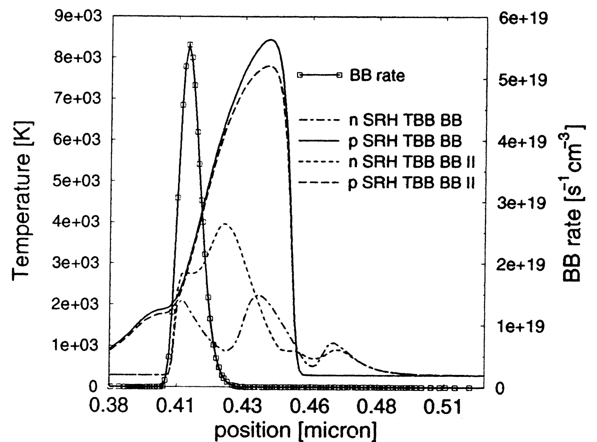

Fig. 8. Carrier heating of the investigated device using an anode (left side) bias of 4 V. The results correspond to model sets, which accounts for the SRH/TBB/BB and SRH/TBB/BB/II processes. The electrons move from the right to the left. The linear shape of the BB generation rate is also shown.

To compare the ionization process at room temperature with the process at 523 K, it is important to analyze the current parts from the applied generation models without the ionization model. At room temperature, the quotient of $I_{D,SRH}$ current and the pure diffusion current I_D is about $I_{D,SRH}/I_D = 92$ at a bias of 4 V. The TBB current is about a factor $I_{D,SRH,TBB}/I_{D,SRH} = 12.4$ higher. The largest current part comes from the BB process, which raises the current further by a factor of about $I_{D,SRH,TBB,BB}/I_{D,SRH,TBB} = 1098$.

At 523 K, the situation is quite different. Again, we analyze the situation without an ionization model. The quotient of the total current and the diffusion current is $I_{D,SRH,TBB,BB}/I_D = 1.06$, when we apply the same bias of 4 V. This means that the carrier temperature distribution inside the junction is determined by the diffusion current, and therefore the shape of the carrier temperature distribution is similar to that in Fig. 6. For this reason, the influence of carrier cooling inside the junction is small. An additional difference is given by the influence of the applied models. As the BB generation stays in the same order of magnitude, the SRH generation increases with the intrinsic concentration n_i in the order of four magnitudes. The TBB current part increases in the same way like the SRH current, because the electric field stays nearly the same as for 298 K. Therefore, the TBB current gives the largest contribution of all generation models.

When we switch on the HD-II model, a current increase by a factor of 1.37 can be observed even at the low bias of 4 V. This strong influence can be explained by the high carrier concentration inside the junction, which is caused by the raised intrinsic concentration. Even at low biases, the high impact generation rates cool down the carrier systems below the breakdown temperature. Note that Fig. 6 is the result without any ionization model. The shape of the carrier temperature distributions is similar to Fig. 6, which demonstrates that the electrons have the higher temperature and start to ionize. The necessary breakdown temperature, which has to be obtained by both carrier systems, and the much higher carrier concentrations are responsible for the higher field dependent leakage current before breakdown starts. It should be noted that with the parameter set in Table 1, the avalanche temperature coefficient $\alpha_T = \Delta V/\Delta T_L = 2.66\ \mathrm{mV\,K^{-1}}$ is reproduced quite well.

During the simulation, the breakdown temperature at 298 K is about 8500 K using a band-gap of 1.08 eV. At 523 K, the breakdown temperature is about 7200 K with a corresponding band gap of 1.02 eV.

5. Conclusion

In this paper, we presented hydrodynamic breakdown simulations of an overvoltage protection structure with an asymmetric pn-junction. The lattice temperature covers a range from 298 to 523 K. It could be shown that within the HD model, the pre-breakdown generation processes are completely different at room temperature compared to the processes at 523 K. This is mainly caused by the field dependent generation processes in combination with an adiabatic cooling of the carriers. These cooling processes are an inherent limit of the HD device simulation if only one energy system is used for each carrier type.

References

[1] Habaš P. Modeling approaches in studying the hot-carrier aging of MOSFETs. Microel Rel 1994;34(11).
[2] Chynoweth AG. Ionization rates for electrons and holes in silicon. Phys Rev 1958;109:1537–40.
[3] Selberherr S. Analysis and simulation of semiconductor devices. New York: Springer, 1984.
[4] Fischetti MV, Laux SE. Monte Carlo analysis of electron transport in small semiconductor devices including band-structure and space-charge effects. Phys Rev B 1988; 38(14):9721–45.
[5] Tang JY, Hess K. Impact ionization of electrons in silicon (steady state). J Appl Phys 1983;54(9):5139–44.
[6] Wang XL, Chandramouli V, Maziar CM, Tasch AF. An efficient multi-band Monte Carlo model with anisotropic impact ionization. In: Int Electron Dev Meet 1992. p. 725–8.
[7] Slotboom JW, Streutker G, Dort MJv, Woerle PH, Pruijmboom A, Gravesteijn DJ. Non-local impact ionization in silicon devices. In: Int Electron Dev Meet 1991. p. 127–30.
[8] Jungemann C, Meinerzhagen B, Decker S, Keith S, Yamaguchi S, Goto H. Is physically sound and predictive modeling of nmos substrate currents possible? In: Solid-State Electron 1998. p. 647–55.
[9] Knaipp M, Simlinger T, Kanert W, Selberherr S. Analysis of leakage currents in smart power devices. In: Baccarani G, Rudan M, editors. 26th Eur Solid State Dev Res Conf Gif-sur-Yvette Cedex, Editions Frontieres, France, 1996. p. 645–8.
[10] Choi W-S, Ahn J-G, Park Y-J, Min H-S, Hwang C-G. A time dependent hydrodynamic device simulator snu-2d with new discretization scheme and algorithm. IEEE Trans Computer-Aided Des 1994;13(7):899–908.
[11] Green MA. Intrinsic concentration, effective densities of states, and effective mass in silicon. J Appl Phys 1990; 67(6):2944–54.
[12] Slotboom JW, de Graaff HC. Measurements of bandgap narrowing in Si bipolar transistors. Solid-State Electron 1976;19:857–62.
[13] Hänsch W. The drift diffusion equation and its application in MOSFET modeling. New York: Springer, 1991.
[14] Kosina H. Simulation des Ladungstransportes in elektronischen Bauelementen mit Hilfeder Monte-Carlo-Methode. Dissertation, Technische Universität Wien, 1992.
[15] Fischetti MV. Monte Carlo simulation of transport in technologically significant semi-conductors of the diamond

and zinc-blende structures – Part I: Homogeneous transport. IEEE Trans Electron Dev 1991;38(3):634–49.
[16] Palankovski V, Gonzales B, Kosina H, Hernandez A, Selberherr S. A new analytical energy relaxation time model for device simulation. Proc Second Int Conf Model Simulat Microsyst 1999. p. 395–8.
[17] Schenk A. A model for the field and temperature dependence of shockley-read-hall lifetimes in silicon. Solid-State Electron 1992;35(11):1585–96.
[18] Hurkx GAM, Klaassen DBM, Knuvers MPG. A new recombination model for device simulation including tunneling. IEEE Trans Electron Dev 1992;39(2): 331–8.
[19] TMA Medici, Two-Dimensional Device Simulation Program, Version 4.0 User's Manual, Technology Modeling Associates, Sunnyvale, CA, 1997.
[20] Quade W, Rudan M, Schöll E. Hydrodynamic simulation of impact-ionization effects in p–n junctions. IEEE Trans Computer-Aided Des 1991;10(10):1287–94.
[21] Quade W, Schöll E, Rudan M. Impact ionization within the hydrodynamic approach to semiconductor transport. Solid-State Electron 1993;36(10):1493–505.